Please cite this article in press as: Soubias et al., Physiological changes in bilayer thickness induced by cholesterol control GPCR rhodopsin function, Biophysical Journal (2023), https://doi.org/10.1016/j.bpj.2022.11.2937

Biophysical Journal
Article

Biophysical Society

Physiological changes in bilayer thickness induced by cholesterol control GPCR rhodopsin function

Olivier Soubias,[1,*] Alexander J. Sodt,[2] Walter E. Teague,[3] Kirk G. Hines,[3] and Klaus Gawrisch[3]
[1]Macromolecular NMR Section, Center for Structural Biology, Center for Cancer Research, NCI, NIH, Frederick, Maryland; [2]Unit on Membrane Chemical Physics, Eunice Kennedy Shriver NICHD, NIH, Bethesda, Maryland; and [3]Section of NMR, Laboratory of Membrane Biochemistry and Biophysics, NIAAA, NIH, Bethesda, Maryland

ABSTRACT We monitored the effect on function of the G-protein-coupled receptor (GPCR) rhodopsin from small, stepwise changes in bilayer thickness induced by cholesterol. Over a range of phosphatidylcholine bilayers with hydrophobic thickness from ≈21 Å to 38 Å, the metarhodopsin-I (MI)/metarhodopsin-II (MII) equilibrium was monitored with UV-visible spectroscopy while ordering of hydrocarbon chains was probed by ^{2}H-NMR. Addition of cholesterol shifted equilibrium toward MII for bilayers thinner than the average length of hydrophobic transmembrane helices (27 Å) and to MI for thicker bilayers, while small bilayer thickness changes within the range of the protein hydrophobic thickness drastically up- or downregulated MII formation. The cholesterol-induced shifts toward MII for thinner membranes correlated with the cholesterol-induced increase of bilayer hydrophobic thickness measured by NMR, consistent with continuum elastic modeling. The energetic penalty of adding cholesterol to thick bilayers caused rhodopsin oligomerization and a shift toward MI. In membranes of physiological thickness, changes in bilayer mechanical properties induced by cholesterol potentiated the interplay between bilayer and protein thickness resulting in large swings of the MI-MII equilibrium. In membrane containing cholesterol, elastic deformations near the protein are a dominant energetic contribution to the functional equilibrium of the model GPCR rhodopsin.

SIGNIFICANCE Membrane cholesterol is an important allosteric modulator of GPCR function, but the mechanisms by which it acts are not completely understood. In this study, we show that formation of the active MII state of the model GPCR rhodopsin can be up- or downregulated by cholesterol depending on the hydrophobic mismatch between the protein and the surrounding bilayer. Based on data from NMR and molecular simulation, we propose a model that could explain how a GPCR could be turned on or off by physiological changes of bilayer properties induced by small changes in cholesterol content in cell membranes.

INTRODUCTION

In recent decades, our understanding of the molecular basis of G-protein-coupled receptor (GPCR) function has greatly advanced. The determination of, by now, over 450 unique GPCR structures by x-ray crystallography and single-particle cryo-electron microscopy (cryo-EM) has led to insight into the molecular details of these receptors, either alone or in complex with their signaling partners (1). The complementation of these structural insights with biophysical techniques (e.g., NMR, single-molecule fluorescence, hydrogen-deuterium exchange mass spectrometry, and computational approaches) and functional studies using lipid nanoparticle systems (2–5) have revealed that GPCRs are highly dynamic, allosteric proteins that sample complex conformational landscapes (6–9). Receptor activation and signaling pathways have been related to such landscapes in a ligand- and effector-dependent manner (10,11). In addition, it is today increasingly appreciated that the membrane environment can significantly influence the thermodynamic and functional equilibrium between the conformational states of a GPCR through protein-lipid interactions (12,13). These interactions range from bulk physical properties of the surrounding lipid bilayer (14,15) to specific and stoichiometric interactions between a receptor and individual lipid molecules (16,17). Among lipids, cholesterol is, perhaps, the most potent modulator of biological membrane physical properties. Increasing cholesterol content substantially raises acyl chain order and increases bilayer

Submitted September 9, 2022, and accepted for publication November 21, 2022.

*Correspondence: soubiaso@mail.nih.gov

Editor: Heiko Heerklotz.
https://doi.org/10.1016/j.bpj.2022.11.2937

Please cite this article in press as: Soubias et al., Physiological changes in bilayer thickness induced by cholesterol control GPCR rhodopsin function, Biophysical Journal (2023), https://doi.org/10.1016/j.bpj.2022.11.2937

hydrophobic thickness. Typically, though not universally, cholesterol increases mechanical stiffness (as expressed by the area compressibility and bending modulus) (18–21). Inverse hexagonal phase experiments indicate that cholesterol prefers negatively curved monolayers (22). Cholesterol also reduces membrane water penetration (23). In multicomponent lipid mixtures, cholesterol induces phase separations and partitions selectively between different coexisting lipid phases (24). The influence of cholesterol on GPCR function appears to be very much receptor dependent, with reports of up- and downregulation. Its nature remains ambiguous as well, whether ascribed to changes in membrane physical properties or binding to specific hydrophobic receptor sites ((25–30) and references therein).

Rhodopsin, the GPCR responsible for dim-light photoreception in vertebrates, remains one of the model GPCRs and, together with the β_2-adrenergic receptor, is largely responsible for our current understanding of GPCR-bilayer interactions. This is because photoactivated rhodopsin exists as a meta-stable lipid-dependent conformational equilibrium between metarhodopsin-I (MI) and several distinct metarhodopsin-II (MII) states, MII_a, MII_b, and $MII_{b\text{-}H+}$, yielding a conformational landscape similar to other class A GPCRs. The equilibrium of rhodopsin can be easily measured by ultraviolet-visible (UV-vis) spectroscopy (31). Differences in protein shape in the equilibrium have been inferred by sensitivity to the lipid environment (15,32). To date, increased cholesterol has been shown to reduce the formation of MII in native rod outer segment disk membranes and in rhodopsin-containing model membranes made with egg-phosphatidylcholine (egg-PC) (33,34). Those experiments prompted the hypothesis that cholesterol inhibits activation by reducing acyl chain flexibility and the free volume in the core of the bilayer. In this study we explore how addition of cholesterol to bilayers of varied acyl chain length affects rhodopsin function. Phosphatidylcholine (PC) bilayers with hydrophobic thickness ranging from 21 Å to 32 Å were doped with increasing concentrations of cholesterol. Doing so, we changed bilayer thickness by increments of ≈0.5–2 Å from 21 Å to 38 Å, ostensibly with increasing mechanical stiffness of the bilayers. We then monitored how those bilayers deform in the presence of rhodopsin by ^{2}H-NMR and followed the influence of those stepwise changes of bilayer properties on rhodopsin function by UV-vis spectroscopy. We show that, contrary to expectations, addition of cholesterol affects the MI-MII equilibrium differently depending on the bilayer hydrophobic thickness surrounding the protein. In short bilayers, cholesterol favors MII by thickening the bilayer commensurate with MII's increased height. On the contrary, cholesterol in thick bilayers increases the energetic penalty of monolayer deformations, promoting oligomerization of the protein, which favors MI. We also show that addition of cholesterol to bilayers of the approximate thickness of rhodopsin results in sharp swings of the MI-MII equilibrium and that MI is strongly stabilized in bilayers hydrophobically matched to its thickness (MI match point) while MII is favored at the MII match point. Molecular simulations of protein-free bilayers indicate the stiffening effect of cholesterol in the various lipid matrices. Simulations of MI and MII over select composition points mirroring the experiment suggest that the deformation of the bilayer around MII near the MI match point is sufficiently severe to cause the anomalous stabilization of MI observed in experiments. This could explain the sensitivity of GPCR function to small changes of cholesterol content in cell membranes.

MATERIALS AND METHODS

Preparation of reconstituted membranes

Sample preparation was carried out in complete darkness. The phospholipids 1-perdeuteriomyristoyl-2-myristoleoyl-*sn*-glycero-3-phosphocholine ($14{:}0_{d27}$-14:1 PC), 1-perdeuteriopalmitoyl-2-palmitoleoyl-*sn*-glycero-3-phosphocholine ($16{:}0_{d31}$-16:1 PC), 1-perdeuteriostearoyl-2-oleoyl-*sn*-glycero-3-phosphocholine ($18{:}0_{d35}$-18:1 PC), and 1-perdeuterioarachidoyl-2-eicosanoyl-*sn*-glycero-3-phosphocholine ($20{:}0_{d39}$-20:1 PC), and cholesterol were obtained from Avanti Polar Lipids (Alabaster, AL).

Rhodopsin was purified from bovine retinas using procedures that were developed in the Litman laboratory (35) and rhodopsin reconstitution was carried out as in (36). The final rhodopsin concentration in the samples was measured by light absorption at 500 nm assuming a molar extinction coefficient at 500 nm of 40,600 M^{-1} cm^{-1}. Lipid concentration was measured by solution ^{1}H-NMR on a small aliquot of sample dissolved in deuterated chloroform: methanol (2:1 v/v) before and after reconstitution. For NMR experiments on dark-adapted rhodopsin, the proteoliposomes were pelleted at 500,000 × *g* and 4°C for 12 h in a TLX-Optima centrifuge (Beckman-Coulter, Fullerton, CA). The pellet was then extruded through porous anodic aluminum oxide (AAO) filters (Anopore; Whatman, Maidstone, UK) with a nominal pore diameter of 0.2 μm and a thickness of 60 μm, which resulted in formation of tubular, rhodopsin-containing bilayers supported by the pore walls of AAO as described previously (37). Extrusion was performed at ambient temperature, which is well above the main phase-transition temperature of $14{:}0_{d27}$-14:1 PC, $16{:}0_{d31}$-16:1 PC, and $18{:}0_{d35}$-18:1 PC, and at 35°C in a heated glovebox for the $20{:}0_{d39}$-20:1 PC membranes. For each experiment, two AAO filters (diameter 25 mm) and one polycarbonate filter (nominal pore size 0.8 μm) were stacked and flushed with several milliliters of piperazine-*N*,*N*′-bis-2-ethanesulfonic acid (PIPES) buffer (10 mM PIPES, 100 mM NaCl, 50 μM diethylenetriamine pentaacetate [pH 7.0]) before extruding the dispersion of proteoliposomes. The 1-mL proteoliposome suspension (1 mg lipid/mL) was then extruded 15 times through the stack of filters at a rate of 0.01 mL/s, resulting in entrapment of multilamellar bilayers inside AAO pores. All but a single tubular bilayer covering the inner AAO pore surface were removed by flushing the filters with 5–10 mL of PIPES buffer at a rate of 0.2 mL s^{-1} as reported earlier (38).

NMR experiments

Solid-state ^{2}H-NMR experiments were carried out on a Bruker DMX500 spectrometer equipped with a flat coil ^{1}H X-probe (Doty Scientific, Columbia, SC) operating at a ^{2}H-NMR resonance frequency of 76.8 MHz. Data were acquired at 37°C with a quadrupolar echo pulse sequence, $d1$-90°_x-τ-90°_y-τ-acq, at a relaxation delay time $d1$ = 250 ms, a 5-μs 90° pulse, a delay time τ = 50 μs, and 200 kHz spectral width. Typically, 150,000 to 200,000 transients were acquired. Order parameter profiles,

Please cite this article in press as: Soubias et al., Physiological changes in bilayer thickness induced by cholesterol control GPCR rhodopsin function, Biophysical Journal (2023), https://doi.org/10.1016/j.bpj.2022.11.2937

mosaic spread of bilayer orientations, and resonance linewidth were determined by fitting the spectra with a program written in Mathcad (PTC, Needham, MA).

The program reported a smoothed order parameter profile of lipid hydrocarbon chains, the orientational distribution function of bilayer normals (assumed to be Gaussian), and the resonance linewidth of all resolved quadrupolar splittings.

Measurement of MII/MI ratio after photoactivation

The equilibrium constant K_{eq} = [MII]/[MI] was determined from rapidly acquired spectra of the MI-MII equilibrium as previously described (39). In brief, vesicles were diluted to a rhodopsin concentration of ≈0.25 mg/mL in PIPES buffer (pH 7.05) and equilibrated at 37°C in a thermally regulated sample holder. A set of four absorption spectra were collected sequentially in an Agilent 8453 diode array spectrophotometer. These included the spectra acquired: 1) after the sample was equilibrated in the dark at 37°C; 2) 3 s after the sample was bleached 15%–20% by a 520-nm flash; 3) 10 min after addition of 30 mM hydroxylamine to convert bleached rhodopsin to opsin and retinal oxime; and 4) after complete bleach of the sample. Individual MI and MII spectra were deconvolved from spectra of their equilibrium mixture; [MI] and [MII] were determined using extinction coefficients at their absorbance maxima of 44,000 and 38,000 cm^{-1}, respectively (40).

Molecular simulation

The simulation force field was CHARMM C36 (41,42). Starting protein conformations for MI and MII were built as in (43). Approximately 87 lipids per leaflet (175 total), either cholesterol, 14:0-14:1 PC, 16:0-16:1 PC, or 18:0-18:1 PC, were built using the workflow from CHARMM-GUI (44). The water layer was ≈18 Å thick on both sides of the bilayer (≈13,000 water molecules). All simulations were run at 310 K and 1 atm isotropic pressure, with the box area maintained at zero surface tension. Particle-mesh Ewald, with an approximately 1 Å grid spacing, was used to compute long-range electrostatics. Force-based switching of Lennard-Jones interactions was applied between 10 and 12 Å. The time step was 2 fs. Initial simulations were run in NAMD. Pressure was maintained with the Langevin piston algorithm, using standard coupling parameters (a piston oscillation period of 50 ps and decay time of 25 ps). Simulations with cholesterol were later extended with AMBER to collect cholesterol enrichment around the proteins more completely. With AMBER, a Monte Carlo semi-isotropic barostat was used to control pressure. Simulations of MI in 14:0–14:1 PC + 15 mol % cholesterol were run for ≈1.8 μs, while all other cholesterol/lipid/rhodopsin simulations were run between 2.6 and 2.9 μs. Lipid traces and leaflet hydrophobic surfaces, indicating the curvature and thickness of the lipids around the protein, are plotted as in (45). The hydrophobic surface is computed by the average height of the CHARMM C36 C23 atom histogrammed radially. The surface is cut off at a radius of 10, below which the surface could not be sampled adequately. For lipid "traces," the average height and radius of each heavy atom of the phospholipid was computed, averaging radially outward. That is, the radius of each atom relative to the center of the mass of the protein is computed and sorted by radius. For a particular frame, averages of the height and radius of the first five of such atoms are computed before moving to the next set of five, yielding shell-by-shell averages of position and height. The shell-based quantities are further averaged over the entire trajectory. Relative enrichment of cholesterol is computed as in (46). In brief, a Voronoi diagram is constructed from the positions of individual lipids and a set of atoms from the protein. The lipid shell is assigned by the number of "hops" away from the central protein—those lipids directly neighboring the protein by Voronoi analysis are assigned to the first shell. Enrichment is computed by dividing the fractional occupancy of cholesterol by the bulk fraction.

RESULTS

Ordering of bilayers of different thickness by cholesterol

We first monitored how cholesterol orders bilayers of different thickness without rhodopsin. To do so, we incorporated cholesterol at mole fraction up to 30 mol % into PC membranes with saturated and perdeuterated *sn*-1 acyl chains and mono-unsaturated *sn*-2 acyl chains of 14, 16, 18, and 20 methylene segments in length. ^{2}H-NMR spectra were acquired at 37°C on single oriented lipid bilayers in the fluid phase supported by porous AAO substrates as described previously (37). Fig. 1 shows the average order parameter of the *sn*-1 chain ($<S^{rho-}>$; here rho$^-$ indicates a bilayer without rhodopsin) as a function of cholesterol concentration for each lipid chain length. Cholesterol raises hydrocarbon chain order regardless of chain length. This is in agreement with cholesterol residing in an upright position among the hydrocarbon chains beneath the lipid headgroups, manifesting in membrane thickening (47). The slope of $<S^{rho-}>$ as a function of cholesterol concentration indicates that longer acyl chains are more susceptible to ordering. This suggests that the tilt of the cholesterol long axis and/or cholesterol wobbling motions differ depending on bilayer thickness. Order increases linearly with cholesterol concentration in 14:0-14:1 PC, 16:0-16:1 PC. and 18:0-18:1 PC bilayers but levels off at 15 mol % cholesterol in 20:0-20:1 PC bilayers. Effective hydrophobic thicknesses obtained as a function of cholesterol concentration for each lipid chain length and calculated as in (36) and references therein changed continuously from 21.0 Å to 23.5 Å for 14:0$_{d27}$-14:1 PC, from 24.6 Å to 29.6 Å for 16:0$_{d27}$-16:1 PC, from 28.3 Å to 33.5 Å for 18:0$_{d27}$-18:1 PC, and from 32.3 Å to 37.5 Å (15 mol % cholesterol) for 20:0$_{d39}$-20:1 PC before plateauing at larger cholesterol concentration (Table S1).

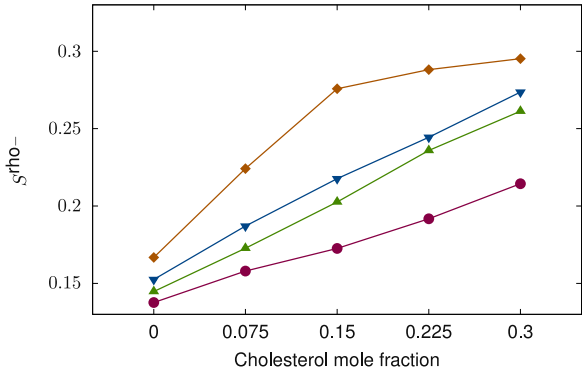

FIGURE 1 Average *sn*-1 chain order parameters ($<S^{rho-}>$) in membranes without rhodopsin as a function of cholesterol mole fraction, measured at 37°C. 14:0$_{d27}$-14:1 PC (*purple circles*), 16:0$_{d31}$-16:1 PC (*green triangles*), 18:0$_{d35}$-18:1 PC (*blue triangles*), and 20:0$_{d39}$-20:1 PC (*brown diamonds*). To see this figure in color, go online.

Please cite this article in press as: Soubias et al., Physiological changes in bilayer thickness induced by cholesterol control GPCR rhodopsin function, Biophysical Journal (2023), https://doi.org/10.1016/j.bpj.2022.11.2937

Deformations of cholesterol-containing bilayers in the presence of rhodopsin

The same series of phospholipid-cholesterol mixtures (except for bilayers with more than 15 mol % cholesterol in 20:0-20:1 PC) was then used to measure changes in order in the presence of rhodopsin (Fig. 2 *A*). To do so, we incorporated dark-adapted rhodopsin at a rhodopsin/lipid ratio of 1:1000. This ratio was chosen because it minimizes receptor oligomerization in pure PC membranes (48).

In rhodopsin-containing membranes, a ^{2}H-NMR experiment will report lipid order, averaged over lipids both near the protein and in the bulk, on a timescale of 10^{-4}–10^{-5} s according to Eq. 1:

$$< S^{\mathrm{rho+}} > \; = \chi_{\mathrm{f}} \; < S^{\mathrm{f}} > \; + \left(1 - \chi_{\mathrm{f}}\right) < S^{\mathrm{b}} > , \qquad (1)$$

where $<S^{\mathrm{f}}>$ is the order parameter of free lipids away from rhodopsin, $<S^{\mathrm{b}}>$ is the order parameter of lipids in the boundary layer surrounding rhodopsin, and χ_{f} is the fraction of free lipids away from rhodopsin. For simplicity, it was assumed that the boundary layer consists of lipid molecules surrounding every rhodopsin molecule as a first layer only, which is a simplification (49,50).

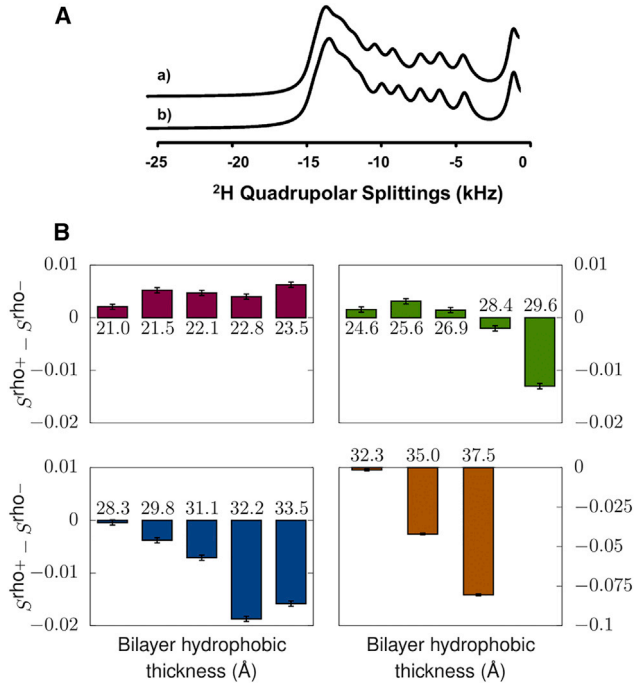

FIGURE 2 (*A*) ^{2}H-NMR spectra of 14:0$_{\mathrm{d27}}$-14:1-PC + 15 mol % cholesterol bilayers (*a*) with rhodopsin at a P/L 1:1000 and (*B*) without rhodopsin (only the left half of the spectra are shown). The AAO-supported sample of tubular lipid bilayers was oriented such that the pores are aligned parallel to the static magnetic field of the NMR instrument, resulting in a preferential perpendicular orientation of the bilayer normal to the magnetic field. (*B*) Difference between average *sn*-1 chain order parameters, $<\Delta S_{\mathrm{diff}}> = <S^{\mathrm{rho+}}> - <S^{\mathrm{rho-}}>$, of 14:0d27-14:1 PC (*top left*, *purple*), 16:0d31-16:1 PC (*top right*, *green*), 18:0d35-18:1 PC (*bottom left*, *blue*), and 20:0d39-20:1 PC (*bottom right*, *brown*) as a function of bilayer hydrophobic thickness of bilayers with increasing cholesterol concentration. Note that the *y*-axis scale for data in 20:0d39-20:1 PC is larger than for data in shorter bilayers. Experiments were conducted at 37°C. Duplicate preparations were analyzed to determine the error for the fitted order parameters. To see this figure in color, go online.

The difference $<\Delta S^{\mathrm{diff}}>$ between the average acyl chain order parameters measured in rhodopsin-containing ($<S^{\mathrm{rho+}}>$) and in rhodopsin-free membranes ($<S^{\mathrm{rho-}}>$) depends on the average order parameter in the boundary layer and on the fraction of boundary lipids ($1 - \chi_{\mathrm{f}}$) according to Eq. 2:

$$\begin{aligned} < \Delta S^{\mathrm{diff}} > \; &= \; < S^{\mathrm{rho+}} > - < S^{\mathrm{rho-}} > \\ &= \; \left(1 - \chi_{\mathrm{f}}\right)\left(< S^{\mathrm{b}} > - < S^{\mathrm{f}} > \right). \end{aligned} \qquad (2)$$

Without oligomerization or lipid demixing, $(1 - \chi_{\mathrm{f}})$ is independent of the lipid composition and $<\Delta S^{\mathrm{diff}}>$ is proportional to the extent of the lipid deformation near the protein. Chain ordering near rhodopsin results in a positive $<\Delta S^{\mathrm{diff}}>$ while disordering results in a negative $<\Delta S^{\mathrm{diff}}>$; if oligomerization occurs, the fraction of lipids that interact the protein $(1 - \chi_{\mathrm{f}})$ is reduced and $<\Delta S^{\mathrm{diff}}>$ decreases. If lipid demixing occurs, $<S_{\mathrm{b}}>$ changes drastically and large $<\Delta S^{\mathrm{diff}}>$ values are expected (see below).

Fig. 2 *B* shows the influence of increasing bilayer thickness by increasing cholesterol concentration on $<\Delta S^{\mathrm{diff}}>$. Rhodopsin increased acyl chain order in membranes thinner than 27 Å ($<\Delta S^{\mathrm{diff}}>$ is positive) and decreased order in thicker membranes ($<\Delta S^{\mathrm{diff}}>$ is negative). The switch from a positive $<\Delta S^{\mathrm{diff}}>$ value to a negative $<\Delta S^{\mathrm{diff}}>$ value occurred between 15 mol % and 22.5 mol % of cholesterol in 16:0-16:1 PC membrane (i.e., between bilayer thickness = 26.9 Å and 28.4 Å, respectively; see Fig. 2 *B*, *top right*). This is in very good agreement with the value of the average rhodopsin hydrophobic thickness of 27 Å determined in pure PC lipid bilayers (48). Noticeably, the magnitude of $<\Delta S^{\mathrm{diff}}>$ is larger in membranes containing cholesterol than in cholesterol-free membranes. In particular, large negative $<\Delta S^{\mathrm{diff}}>$ values are observed in bilayers of hydrophobic thickness of 30 Å and upward (Fig. 2 *B*, *bottom left and right*), with values ranging from −0.005 to −0.1 when averaged over all lipids. This corresponds to a much larger reduction in thickness than would be expected from hydrophobic matching when converted to a change in only the first layer (≈25 lipids). For instance, the $<\Delta S^{\mathrm{diff}}>$ observed in 18:0-18:1 PC and 15 mol % cholesterol (−0.007) would correspond to a thickness of ≈18 Å in the first layer surrounding rhodopsin, much smaller than the protein thickness. Measurement of ratios between lipids and rhodopsin validated that the final lipid sample composition of membranes with and without rhodopsin was identical within experimental error. Hence, such reductions indicate lateral separation of cholesterol and lipids, which is by formation of rhodopsin/cholesterol oligomeric clusters.

Please cite this article in press as: Soubias et al., Physiological changes in bilayer thickness induced by cholesterol control GPCR rhodopsin function, Biophysical Journal (2023), https://doi.org/10.1016/j.bpj.2022.11.2937

Cholesterol up- or downregulates MII formation depending on membrane thickness

The influence of changes in bilayer thickness on rhodopsin function was then followed by measurements of the MI/MII equilibrium (K_{eq} = MII/MI) by UV-vis spectroscopy. Assuming a Boltzmann distribution, the logarithm of K_{eq} is proportional to the difference in free energies between the photointermediates MII and MI, $\Delta\Delta G^{(MI \rightarrow MII)} \propto \ln K_{eq}$. The experimental results are reported in Fig. 3. Increasing cholesterol concentration in 14:0-14:1 PC bilayers raised the MII concentration while adding cholesterol to either 18:0-18:1 or 20:0-20:1 PC membranes shifted the equilibrium toward the inactive MI. Of particular interest were the changes over the physiological relevant thickness range of 26–29 Å where the results were more complex and measured with smaller increments of cholesterol. For 16:0-16:1 PC and cholesterol concentrations in the membrane from 0 to 18.75 mol %, a rapid decrease of $\ln K_{eq}$ was observed. Then, from 18.75 to 30 mol %, $\ln K_{eq}$ increased rapidly. The fraction of MII formed after photoactivation goes from 0.53 in 16:0-16:1 PC to 0.45 in bilayers containing 18.75 mol % of cholesterol before rising back to 0.62 at 30 mol % cholesterol, i.e., within ≈3 Å. For comparison, the fraction of MII formed in 14:0-14:1 PC and 18:0-18:1 PC (i.e., within ≈8 Å) is 0.48 and 0.62, respectively. Additional experiments were then performed by adding cholesterol to di-unsaturated 16:1-16:1 PC. Fig. 4 shows that a biphasic behavior is also observed in those bilayers. The minimum is shifted to slightly higher cholesterol concentration (22.5 mol %), consistent with unsaturated hydrocarbon chains being less thick than mixed saturated/unsaturated chains of equal hydrocarbon chain length. Therefore, this suggests that a complex interplay between bilayer thickness, bilayer stiffness, and rhodopsin conformations may be responsible for the up- and downregulation of MII formation.

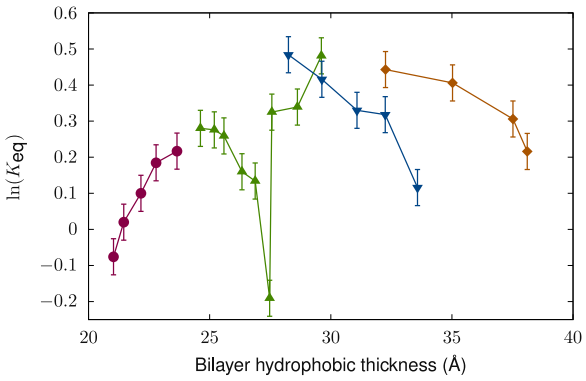

FIGURE 3 Natural logarithm of the ratio of concentrations of photointermediates MII and MI, $\ln K_{eq} = \ln[MII]/[MI]$ as a function of bilayer hydrophobic thickness modulated by cholesterol concentration. 14:0-14:1 PC (*purple circles*, cholesterol mole fraction 0, 0.075, 0.15, 0.225, and 0.3 from left to right), 16:0-16:1 PC (*green triangles*, cholesterol mole fraction 0, 0.075, 0.15, 0.225, and 0.3 from left to right), 18:0-18:1 PC (*blue triangles*, cholesterol mole fraction 0, 0.0375, 0.075, 0.1125, 0.15, 0.1825, 0.225, 0.2625, and 0.3 from left to right), and 20:0-20:1 PC (*brown diamonds*, cholesterol mole fraction 0, 0.075, 0.15, and 0.225 from left to right). Rhodopsin/lipid ratio was 1:1000. Data are expressed as means ± SD from triplicate experiments measured on the same preparation. Data from at least two independent preparations were analyzed. To see this figure in color, go online.

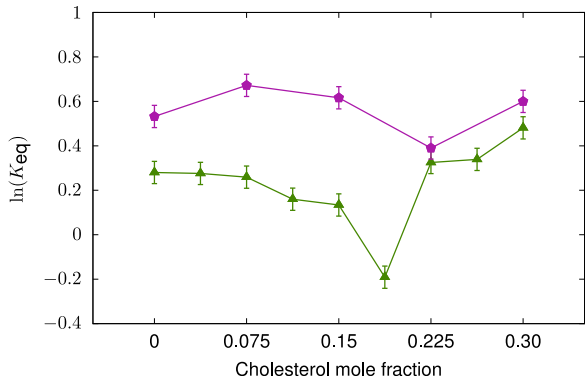

FIGURE 4 Natural logarithm of the MII/MI ratio as a function of the mole fraction of cholesterol in 16:1-16:1 PC bilayers (*purple symbols*). Hydrophobic thickness of bilayers composed of lipids with two unsaturated hydrocarbon chains is slightly lower compared with thickness of mixed saturated/unsaturated chain bilayers of equal hydrocarbon chain length. For comparison, data obtained in 16:0-16:1 PC bilayers are also shown (*green triangles*). Data are expressed as means ± SD from triplicate experiments measured on the same preparation. Data from two independent preparations were analyzed. To see this figure in color, go online.

Molecular simulations indicate cholesterol depletion near rhodopsin

Fig. 5 reports the depletion of cholesterol near rhodopsin reported from all-atom simulations in five different conditions (14:0-14:1 PC + 15 mol % cholesterol, 14:0-14:1 PC + 30 mol % cholesterol, 16:0-16:1 PC + 15 mol % cholesterol, 16:0-16:1 PC + 30 mol % cholesterol, and 18:0-18:1 PC + 15 mol % cholesterol). Cholesterol in the first shell is nearly equivalent to bulk for the thinnest bilayer (14:0-14:1 PC + 15 mol % cholesterol) and decreases as the thicker bulk becomes favorable for cholesterol. Generally cholesterol favors MII, presumably because of its increased height. As discussed below, the anomalous increase in cholesterol enrichment of MI relative to MII for bilayers close to the MI match point is consistent with the anomalous stabilization of MI observed experimentally.

DISCUSSION

Previous work has shown that rhodopsin packs at lowest membrane perturbation in pure PC bilayers with a hydrophobic thickness of 27 ± 1 Å and that mismatch-induced curvature stress favors the formation of MII in thicker membranes (48). Here, we investigated how addition of cholesterol affects function in bilayers that are shorter than, thicker than, or matched to rhodopsin. To do so, we combined functional data obtained by UV-vis spectroscopy

Please cite this article in press as: Soubias et al., Physiological changes in bilayer thickness induced by cholesterol control GPCR rhodopsin function, Biophysical Journal (2023), https://doi.org/10.1016/j.bpj.2022.11.2937

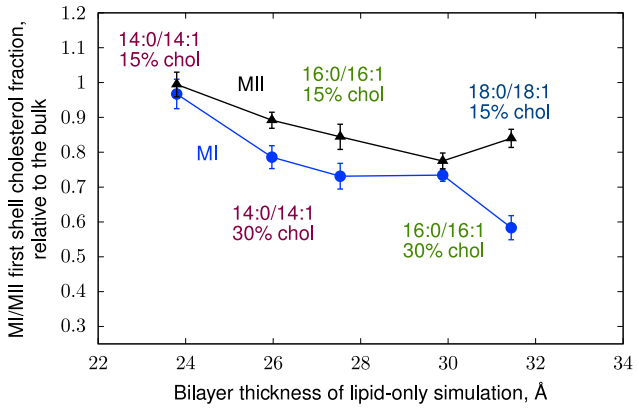

FIGURE 5 Relative enrichment of cholesterol in the first shell of rhodopsin as computed by molecular simulation. Relative enrichment is the fraction of cholesterol observed in the first shell near the protein divided by the mole fraction in the whole bilayer. Error bars are one standard error of the mean computed from at least twelve blocks of 100 nanoseconds. To see this figure in color, go online.

with structural data obtained by solid-state ^{2}H-NMR and computational approaches.

Addition of cholesterol to thin bilayers favors MII

For bilayers much shorter than the average height of rhodopsin (e.g., 14:0-14:1 PC), addition of cholesterol favors formation of the active MII state (Fig. 3). This is consistent with the expectation that cholesterol's preference for negatively curved monolayers and its membrane-thickening properties reduce curvature-elastic energy upon MII formation (12,13) (Fig. 6, *B* and *C*). The monotonic increase of MII with increasing bilayer thickness implies that cholesterol does not drastically influence the elastic properties of 14:0-14:1 PC bilayers. This is consistent with the smaller ordering power observed by ^{2}H-NMR (Fig.1) and the smaller calculated increase in bending elasticity (Table S2).

Addition of cholesterol to thick bilayers favors MI

Increasing the thickness of bilayers beyond rhodopsin (e.g., 18:0-18:1 PC and 20:0-20:1 PC) by adding cholesterol favors MI, in opposition to the well-established model for rhodopsin monomers ((48) and Fig. 6, *A* and *B*). Instead, this is consistent with the induction of rhodopsin oligomerization, as supported by our ^{2}H-NMR data (Fig. 2 *B*, *lower panels*). Rhodopsin clustering in response to the energetic constraints of a hydrophobic mismatch between lipids and protein was reported previously. A chain-length dependence of protein oligomerization was observed experimentally by Ryba and Marsh (51), Kusumi et al. (52), Botelho et al. (53), and Soubias et al. (48), and with coarse-grained molecular dynamics by Periole et al. (54). Our previous study in pure PC membranes showed that the onset of protein oligomerization occurs at a much higher protein concentration, but previous work has suggested that cholesterol increases the penalty for membrane deformation under negative mismatch, promoting peptide segregation (55). It is therefore not entirely surprising that rhodopsin oligomerization occurs at much lower protein concentration in membranes containing cholesterol. It is possible that the reduction in MII formation upon addition of cholesterol in egg-PC model membranes (which are mostly composed of lipids with acyl chains of 18 carbons in length) was also due to rhodopsin clustering. Rates, on the other hand, should solidly depend on chain ordering (36,56). In bovine disk membranes, cholesterol is present at 5–30 mol %, depending on the age of the disk. Competent disks have the lowest cholesterol concentration. From the results described here, it is possible that rhodopsin clusters would be present in newly formed disks before gradually disappearing upon disk maturation.

Complex equilibrium in bilayers nearly matched to rhodopsin

Variation of the MI-MII equilibrium in 16:0-16:1 PC + cholesterol is again inconsistent with the homogeneous elastic membrane model that predicts a monotonic stabilization of MII with increasing bilayer thickness. The sharp change in the MI population upon addition of cholesterol to 16:0-16:1 PC bilayers suggests a mechanism coupling a rapid change of bilayer elastic properties to elastic deformations near MI and MII. MI is sharply favored in bilayers of hydrophobic thickness $\approx$27.5 Å, close to the average thickness of rhodopsin (i.e., the MI match point). When cholesterol is further increased, the stability of MII increases rapidly.

Increasing stiffness over a range of thickness spanning the match points of both MI and MII (i.e., when bilayer deformations are minimal near MI or MII) could lead to sharply nonlinear variation of the equilibrium. Near the match point of MI, when the deformation of MII is greater, stiffening destabilizes MII. Increasing thickness and mechanical stiffness of the bilayer rapidly leads to the relative stabilization of MII as the thickness of MI is surpassed by the matrix. A corollary is that the concentration of cholesterol near hydrophobic match points will reflect the energetics of the deformation: Depletion of cholesterol in a deformed bilayer lowers the cost of the deformation. From the logic of Fig. 6, near the match point of MI, cholesterol will be anomalously enriched near MI relative to MII. As thickness increases, the reverse will hold and cholesterol will be depleted from MI. That is, cholesterol enrichment is mirroring the stability of MI or MII.

While simulations cannot yet quantitatively sample the equilibrium between MI and MII, for which the timescale of interchange is not practical to sample, they can indicate the membrane deformation around the two structures. Fig. S1 shows the hydrophobic surface around MI and MII for the 14:0-14:1 PC lipid matrix, including lipid traces indicating the orientation of nearby lipids. The simulations hint at the increased averaged thickness of

Please cite this article in press as: Soubias et al., Physiological changes in bilayer thickness induced by cholesterol control GPCR rhodopsin function, Biophysical Journal (2023), https://doi.org/10.1016/j.bpj.2022.11.2937

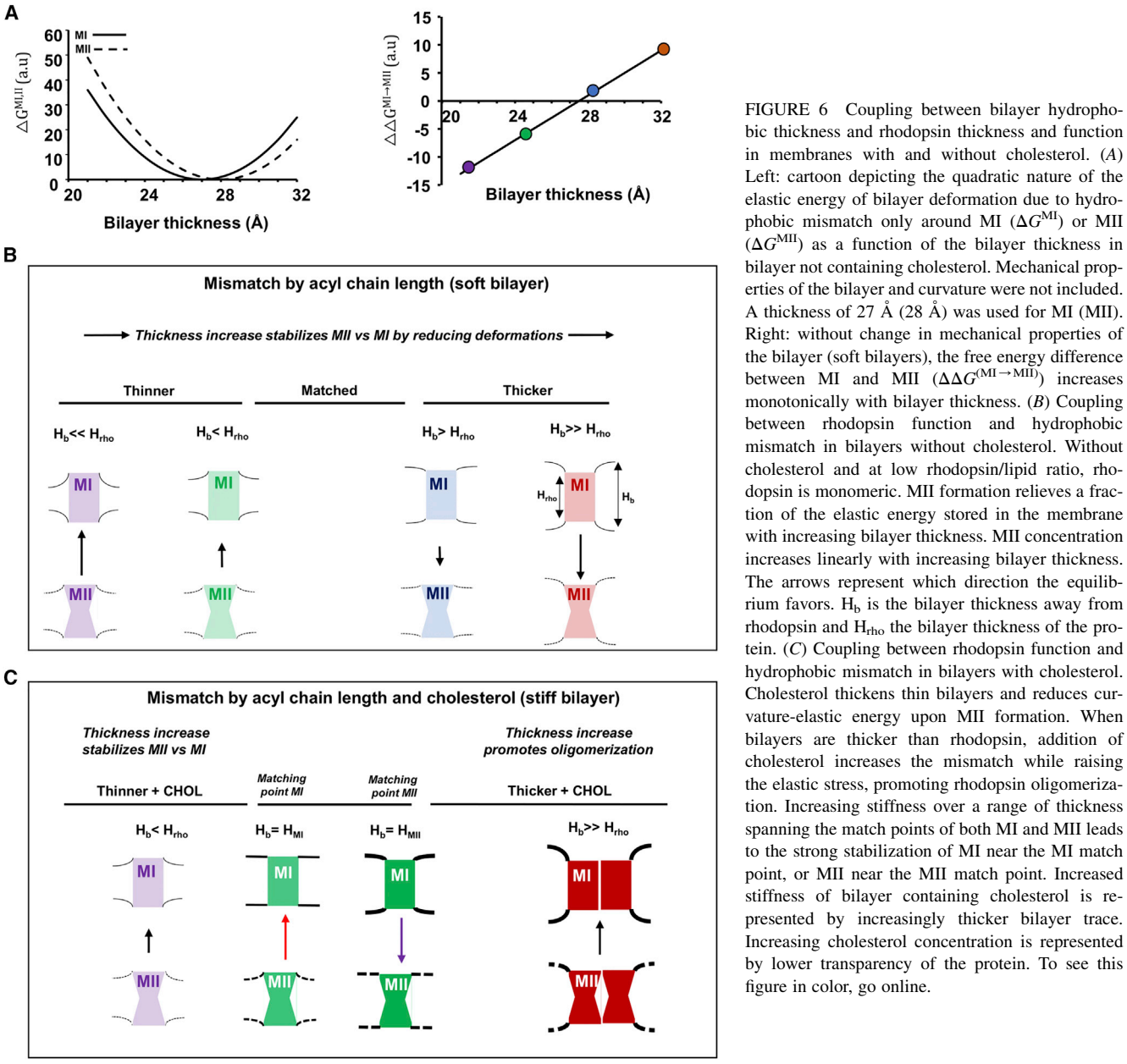

FIGURE 6 Coupling between bilayer hydrophobic thickness and rhodopsin thickness and function in membranes with and without cholesterol. (*A*) Left: cartoon depicting the quadratic nature of the elastic energy of bilayer deformation due to hydrophobic mismatch only around MI (ΔG^{MI}) or MII (ΔG^{MII}) as a function of the bilayer thickness in bilayer not containing cholesterol. Mechanical properties of the bilayer and curvature were not included. A thickness of 27 Å (28 Å) was used for MI (MII). Right: without change in mechanical properties of the bilayer (soft bilayers), the free energy difference between MI and MII ($\Delta\Delta G^{(MI\rightarrow MII)}$) increases monotonically with bilayer thickness. (*B*) Coupling between rhodopsin function and hydrophobic mismatch in bilayers without cholesterol. Without cholesterol and at low rhodopsin/lipid ratio, rhodopsin is monomeric. MII formation relieves a fraction of the elastic energy stored in the membrane with increasing bilayer thickness. MII concentration increases linearly with increasing bilayer thickness. The arrows represent which direction the equilibrium favors. H_b is the bilayer thickness away from rhodopsin and H_{rho} the bilayer thickness of the protein. (*C*) Coupling between rhodopsin function and hydrophobic mismatch in bilayers with cholesterol. Cholesterol thickens thin bilayers and reduces curvature-elastic energy upon MII formation. When bilayers are thicker than rhodopsin, addition of cholesterol increases the mismatch while raising the elastic stress, promoting rhodopsin oligomerization. Increasing stiffness over a range of thickness spanning the match points of both MI and MII leads to the strong stabilization of MI near the MI match point, or MII near the MII match point. Increased stiffness of bilayer containing cholesterol is represented by increasingly thicker bilayer trace. Increasing cholesterol concentration is represented by lower transparency of the protein. To see this figure in color, go online.

MII, although the surface has been averaged around the asymmetric protein. In simulation, the first shell fraction of cholesterol can be quantitatively sampled given the multiple-microsecond trajectories computed here. Roughly mirroring the experiments by scanning over lipid matrix thickness, simulations indicate that cholesterol is depleting from the first shell of both MI and MII as the thicker bulk becomes more favorable for cholesterol (Fig. 5). Preceding 16:0-16:1 PC + 30 mol % cholesterol, the variation is roughly linear, consistent with a linear increase in the stability of MII. Near 16:0-16:1 PC + 30 mol % cholesterol, the enrichment near the shorter MI unexpectedly edges toward MII before dropping off precipitously at 18:0-18:1 PC + 15 mol % cholesterol. The increased enrichment of cholesterol around MI near the match point is consistent with cholesterol's stiffening effect on material properties—when the deformation becomes small, there is little penalty to cholesterol enrichment. While the shift in cholesterol enrichment appears small (expecting perhaps 20% cholesterol in the first shell for MI instead of 22%), the shift reflects an energetic change balancing the entropy:

$$F_{\text{entropy}} = N_{\text{first}}kT\left[\chi_{\text{first}}\ln\left(\frac{\chi_{\text{first}}}{\chi_0}\right) - \left(1-\chi_{\text{first}}\right)\ln\left(\frac{1-\chi_{\text{first}}}{1-\chi_0}\right)\right].$$

Please cite this article in press as: Soubias et al., Physiological changes in bilayer thickness induced by cholesterol control GPCR rhodopsin function, Biophysical Journal (2023), https://doi.org/10.1016/j.bpj.2022.11.2937

For example, with a 30 mol % cholesterol matrix and 40 first shell lipids, the difference in entropic free energy between 22% and 20% first shell cholesterol is −0.4 kT, roughly consistent with the experimental anomaly at the match point. The implication of the simulation is thus that the deformation energy of the first shell lipids near MII is increased relative to MI, near the MI match point. While the simulation condition of maximum enrichment of cholesterol near MI does not precisely match the sharply defined experimentally determined composition favoring MI (at 18.75 mol % cholesterol), the conditions are not precisely equivalent (e.g., the simulation protein/lipid ratio is approximately five times higher), the precise location of the simulation-modeled matching point may be between the simulated values of 15 and 30 mol % cholesterol and the observation is likely sensitive to variations in the elastic properties set by the model force field.

Simulations of binary cholesterol/lipid mixtures without protein indicate qualitatively that the matrix is becoming increasingly stiff but that the dynamic redistribution of cholesterol enhances fluctuations, making the bilayer appear softer. The universal stiffening effect of cholesterol is currently controversial, with equilibrium techniques (such as x-ray diffraction) showing no apparent stiffening of 18:1-18:1 PC (19), while short-wavelength, kinetically determined techniques indicating stiffening (21). We take the view that to completely consider the free energy of the deformation, it is the bending moduli with cholesterol "frozen" (e.g., not considering the undulations induced by its curvature-coupled diffusion (57,58)) that must be considered. This is discussed further in the supporting material. Bending moduli are challenging to quantify, and various methods have been proposed. Applying our methodology, in which the neutral surface, spontaneous curvature differences between lipids, and the bending modulus are simultaneously quantified (59), we find that the bending modulus increases by approximately a factor of two with the addition of 30 mol % cholesterol once the effect of the dynamic redistribution of cholesterol is adjusted for. Relative increases in the bending modulus are reported in the supporting material. It is not wholly necessary to rely on our interpretation of the bending modulus, which may be controversial. X-ray diffraction indicates, for example, that 18:0-18:1 PC is stiffened by cholesterol over the range considered here (19).

Experimental data and simulations show that changes in bulk membrane properties induced by cholesterol potentiate the effect of elastic deformations near the protein to explain the feature of the MI-MII equilibrium. Since the activation pathway of class A GPCR is conserved, it is attractive to extrapolate that the energetic coupling between bilayer and protein thickness could be a strong determinant of the energetic landscape for other members of the family. Nevertheless, many crystal and cryo-EM structures of GPCRs show specific sites for cholesterol or cholesterol derivative interaction, summarized in (60) and references therein. Those observations have prompted the possibility that specific interactions between cholesterol and hotspots on a GPCR could stabilize a particular conformation, as shown for the serotonin 1A receptor (61,62). The systematic functional studies obtained in lipid bilayers as a function of cholesterol concentration presented here do not support bound cholesterol as a dominant mechanism controlling rhodopsin MI-MII equilibrium. Rather, the monotonic dependence of effects and the strong correlation between hydrophobic mismatch and function point to the dominant contribution of elastic deformations near the protein in controlling rhodopsin function. The window for optimal membrane thickness for MII formation is 28–29 Å. Optimal hydrophobic matching remains a crucial determinant for membrane protein function as shown recently for the rhomboid protease GlpG function (63). This makes protein hydrophobic thickness and its measurement critical parameters for interpreting the influence of cholesterol on membrane protein function.

A word of caution needs to be added regarding rhodopsin molecules in reconstituted proteoliposomes. Contrary to rhodopsin in cell membranes, orientation in reconstituted bilayers is likely to be random. It is therefore possible that a random orientation of rhodopsin molecules affects the propensity of rhodopsin to oligomerize. Interpreting mechanical properties of the first lipid solvation shell near proteins is not nearly as well established as a model of pure bilayer elasticity. Furthermore, molecular simulations clearly suggested that the length of hydrophobic segments on rhodopsin is heterogeneous about the circumference of the molecule (54). This has consequences for the energetics of lipid-protein interactions that may not be captured in our simulations.

CONCLUSIONS

Here, we show that membrane cholesterol affects rhodopsin function differently depending on the degree of hydrophobic mismatch. Cholesterol promotes rhodopsin oligomerization in thick membranes and increases formation of the active MII state in thin membranes, apparently with material properties of cholesterol-containing bilayers being a dominant energetic contribution. In membranes of physiological thickness, where bilayer and protein thickness are "matched," we show that a small, local variation in cholesterol concentration can result in large swings of rhodopsin function. We identify elastic deformations near the protein as the main determinant of the energetic landscape of rhodopsin. We envision that systematic studies merging functional and structural data will further our understanding of the role of the lipid bilayer in fine-tuning the function of GPCRs and other membrane proteins.

SUPPORTING MATERIAL

Supporting material can be found online at https://doi.org/10.1016/j.bpj.2022.11.2937.

AUTHOR CONTRIBUTIONS

O.S., A.J.S., and K.G. designed the research. O.S., A.J.S., A.G., W.E.T., and K.G.H. performed the research. O.S. and A.J.S. analyzed the data. O.S. and A.J.S. wrote the manuscript.

ACKNOWLEDGMENTS

This study is dedicated to K.G., highlighting his great contributions to our understanding of the functional role of membranes to cellular function by combining multiple approaches. A.J.S. thanks Klaus for his extraordinary generosity of mentorship and support. O.S. deeply thanks Klaus for sharing his nearly limitless knowledge of membrane biophysics with him and for having not only been a key and kind mentor throughout his scientific career, but also a dear friend who witnessed many of his life-changing moments.

This work was supported by the Intramural Research Program of NIAAA (O.S., W.E.T., K.G.H., and K.G.), NCI (O.S.), and NICHD (A.J.S.). Prof. Alan Grossfield is thanked for gracefully sharing all-atom molecular dynamics simulations of MI and MII. This work utilized the computational resources of the NIH HPC Biowulf cluster.

DECLARATION OF INTERESTS

The authors declare no competing interests.

REFERENCES

1. Weis, W. I., and B. K. Kobilka. 2018. The molecular basis of G protein-coupled receptor activation. *Annu. Rev. Biochem.* 87:897–919. https://doi.org/10.1146/annurev-biochem-060614-033910. https://www.ncbi.nlm.nih.gov/pubmed/29925258.
2. Lavington, S., and A. Watts. 2020. Lipid nanoparticle technologies for the study of G protein-coupled receptors in lipid environments. *Biophys. Rev.* https://doi.org/10.1007/s12551-020-00775-5. https://www.ncbi.nlm.nih.gov/pubmed/33215301.
3. McLean, M. A., M. C. Gregory, and S. G. Sligar. 2018. Nanodiscs: a controlled bilayer surface for the study of membrane proteins. *Annu. Rev. Biophys.* 47:107–124. https://doi.org/10.1146/annurev-biophys-070816-033620. https://www.ncbi.nlm.nih.gov/pubmed/29494254.
4. Soubias, O. 2021. Squaring off with G protein-coupled receptors function in polymer nanoscale lipid bilayers. *Biophys. J.* 120:4299–4300. https://doi.org/10.1016/j.bpj.2021.09.013. https://www.ncbi.nlm.nih.gov/pubmed/34537110.
5. Gunsel, U., and F. Hagn. 2022. Lipid nanodiscs for high-resolution NMR studies of membrane proteins. *Chem. Rev.* 122:9395–9421. https://doi.org/10.1021/acs.chemrev.1c00702. https://www.ncbi.nlm.nih.gov/pubmed/34665588.
6. Latorraca, N. R., A. J. Venkatakrishnan, and R. O. Dror. 2017. GPCR dynamics: structures in motion. *Chem. Rev.* 117:139–155. https://doi.org/10.1021/acs.chemrev.6b00177. https://www.ncbi.nlm.nih.gov/pubmed/27622975.
7. Picard, L. P., and R. S. Prosser. 2021. Advances in the study of GPCRs by (19)F NMR. *Curr. Opin. Struct. Biol.* 69:169–176. https://doi.org/10.1016/j.sbi.2021.05.001. https://www.ncbi.nlm.nih.gov/pubmed/34130235.
8. Periole, X. 2017. Interplay of G Protein-Coupled receptors with the membrane: insights from supra-atomic Coarse grain molecular dynamics simulations. *Chem. Rev.* 117:156–185. https://doi.org/10.1021/acs.chemrev.6b00344. https://www.ncbi.nlm.nih.gov/pubmed/28073248.
9. Hilger, D. 2021. The role of structural dynamics in GPCR-mediated signaling. *FEBS J.* 288:2461–2489. https://doi.org/10.1111/febs.15841. https://www.ncbi.nlm.nih.gov/pubmed/33871923.
10. Deupi, X., and B. Kobilka. 2007. Activation of G protein-coupled receptors. *Adv. Protein Chem.* 74:137–166. https://doi.org/10.1016/S0065-3233(07)74004-4. https://www.ncbi.nlm.nih.gov/pubmed/17854657.
11. Deupi, X., and B. K. Kobilka. 2010. Energy landscapes as a tool to integrate GPCR structure, dynamics, and function. *Physiology.* 25:293–303. https://doi.org/10.1152/physiol.00002.2010. https://www.ncbi.nlm.nih.gov/pubmed/20940434.
12. Brown, M. F. 2017. Soft matter in lipid-protein interactions. *Annu. Rev. Biophys.* 46:379–410. https://doi.org/10.1146/annurev-biophys-070816-033843. https://www.ncbi.nlm.nih.gov/pubmed/28532212.
13. Soubias, O., and K. Gawrisch. 2012. The role of the lipid matrix for structure and function of the GPCR rhodopsin. *Biochim. Biophys. Acta.* 1818:234–240. https://doi.org/10.1016/j.bbamem.2011.08.034. https://www.ncbi.nlm.nih.gov/pubmed/21924236.
14. Fried, S. D. E., J. W. Lewis, …, M. F. Brown. 2021. Membrane curvature revisited-the archetype of rhodopsin studied by time-resolved electronic spectroscopy. *Biophys. J.* 120:440–452. https://doi.org/10.1016/j.bpj.2020.11.007. https://www.ncbi.nlm.nih.gov/pubmed/33217383.
15. Soubias, O., W. E. Teague, Jr., …, K. Gawrisch. 2010. Contribution of membrane elastic energy to rhodopsin function. *Biophys. J.* 99:817–824. https://doi.org/10.1016/j.bpj.2010.04.068. https://www.ncbi.nlm.nih.gov/pubmed/20682259.
16. Soubias, O., W. E. Teague, and K. Gawrisch. 2006. Evidence for specificity in lipid-rhodopsin interactions. *J. Biol. Chem.* 281:33233–33241. https://doi.org/10.1074/jbc.M603059200. https://www.ncbi.nlm.nih.gov/pubmed/16959786.
17. Yen, H. Y., K. K. Hoi, …, C. V. Robinson. 2018. PtdIns(4,5)P2 stabilizes active states of GPCRs and enhances selectivity of G-protein coupling. *Nature.* 559:423–427. https://doi.org/10.1038/s41586-018-0325-6. https://www.ncbi.nlm.nih.gov/pubmed/29995853.
18. Chen, Z., and R. P. Rand. 1997. The influence of cholesterol on phospholipid membrane curvature and bending elasticity. *Biophys. J.* 73:267–276. https://doi.org/10.1016/S0006-3495(97)78067-6. https://www.ncbi.nlm.nih.gov/pubmed/9199791.
19. Pan, J. J., T. T. Mills, …, J. F. Nagle. 2009. Cholesterol perturbs lipid bilayers non-universally. *Biophys. J.* 96:161a.
20. Nagle, J. F. 2021. Measuring the bending modulus of lipid bilayers with cholesterol. *Phys. Rev. E.* 104:044405. https://doi.org/10.1103/PhysRevE.104.044405. https://www.ncbi.nlm.nih.gov/pubmed/34781561.
21. Chakraborty, S., M. Doktorova, …, R. Ashkar. 2020. How cholesterol stiffens unsaturated lipid membranes. *Proc. Natl. Acad. Sci. USA.* 117:21896–21905. https://doi.org/10.1073/pnas.2004807117. https://www.ncbi.nlm.nih.gov/pubmed/32843347.
22. Kollmitzer, B., P. Heftberger, …, G. Pabst. 2013. Monolayer spontaneous curvature of raft-forming membrane lipids. *Soft Matter.* 9:10877–10884. https://doi.org/10.1039/C3SM51829A. https://www.ncbi.nlm.nih.gov/pubmed/24672578.
23. Subczynski, W. K., A. Wisniewska, …, A. Kusumi. 1994. Hydrophobic barriers of lipid bilayer membranes formed by reduction of water penetration by alkyl chain unsaturation and cholesterol. *Biochemistry.* 33:7670–7681. https://doi.org/10.1021/bi00190a022. https://www.ncbi.nlm.nih.gov/pubmed/8011634.
24. Feigenson, G. W. 2006. Phase behavior of lipid mixtures. *Nat. Chem. Biol.* 2:560–563. https://doi.org/10.1038/nchembio1106-560. https://www.ncbi.nlm.nih.gov/pubmed/17051225.
25. Oates, J., B. Faust, …, A. Watts. 2012. The role of cholesterol on the activity and stability of neurotensin receptor 1. *Biochim. Biophys. Acta.* 1818:2228–2233. https://doi.org/10.1016/j.bbamem.2012.04.010. https://www.ncbi.nlm.nih.gov/pubmed/22551944.
26. Oates, J., and A. Watts. 2011. Uncovering the intimate relationship between lipids, cholesterol and GPCR activation. *Curr. Opin. Struct. Biol.* 21:802–807. https://doi.org/10.1016/j.sbi.2011.09.007. https://www.ncbi.nlm.nih.gov/pubmed/22036833.
27. Paila, Y. D., and A. Chattopadhyay. 2009. The function of G-protein coupled receptors and membrane cholesterol: specific or general

interaction? *Glycoconj. J.* 26:711–720. https://doi.org/10.1007/s10719-008-9218-5. https://www.ncbi.nlm.nih.gov/pubmed/19052861.

28. Paila, Y. D., and A. Chattopadhyay. 2010. Membrane cholesterol in the function and organization of G-protein coupled receptors. *Subcell. Biochem.* 51:439–466. https://doi.org/10.1007/978-90-481-8622-8_16. https://www.ncbi.nlm.nih.gov/pubmed/20213554.

29. Paila, Y. D., S. Tiwari, and A. Chattopadhyay. 2009. Are specific nonannular cholesterol binding sites present in G-protein coupled receptors? *Biochim. Biophys. Acta.* 1788:295–302. https://doi.org/10.1016/j.bbamem.2008.11.020. https://www.ncbi.nlm.nih.gov/pubmed/19111523.

30. Serdiuk, T., M. Manna, …, D. J. Muller. 2022. A cholesterol analog stabilizes the human beta2-adrenergic receptor nonlinearly with temperature. *Sci. Signal.* 15:eabi7031. https://doi.org/10.1126/scisignal.abi7031. https://www.ncbi.nlm.nih.gov/pubmed/35671340.

31. Brown, M. F. 2012. UV-visible and infrared methods for investigating lipid-rhodopsin membrane interactions. *Methods Mol. Biol.* 914:127–153. https://doi.org/10.1007/978-1-62703-023-6_8. https://www.ncbi.nlm.nih.gov/pubmed/22976026.

32. Brown, M. F. 1994. Modulation of rhodopsin function by properties of the membrane bilayer. *Chem. Phys. Lipids.* 73:159–180. https://doi.org/10.1016/0009-3084(94)90180-5. https://www.ncbi.nlm.nih.gov/pubmed/8001180.

33. Mitchell, D. C., M. Straume, …, B. J. Litman. 1990. Modulation of metarhodopsin formation by cholesterol-induced ordering of bilayer lipids. *Biochemistry.* 29:9143–9149. https://doi.org/10.1021/bi00491a007. https://www.ncbi.nlm.nih.gov/pubmed/2271584.

34. Niu, S. L., D. C. Mitchell, and B. J. Litman. 2002. Manipulation of cholesterol levels in rod disk membranes by methyl-beta-cyclodextrin: effects on receptor activation. *J. Biol. Chem.* 277:20139–20145. https://doi.org/10.1074/jbc.M200594200. https://www.ncbi.nlm.nih.gov/pubmed/11889130.

35. Litman, B. J. 1982. Purification of rhodopsin by concanavalin A affinity chromatography. *Methods Enzymol.* 81:150–153. https://doi.org/10.1016/s0076-6879(82)81025-2. https://www.ncbi.nlm.nih.gov/pubmed/7098858.

36. Soubias, O., S. L. Niu, …, K. Gawrisch. 2008. Lipid-rhodopsin hydrophobic mismatch alters rhodopsin helical content. *J. Am. Chem. Soc.* 130:12465–12471. https://doi.org/10.1021/ja803599x. https://www.ncbi.nlm.nih.gov/pubmed/18712874.

37. Soubias, O., I. V. Polozov, …, K. Gawrisch. 2006. Functional reconstitution of rhodopsin into tubular lipid bilayers supported by nanoporous media. *Biochemistry.* 45:15583–15590. https://doi.org/10.1021/bi061416d. https://www.ncbi.nlm.nih.gov/pubmed/17176079.

38. Gaede, H. C., K. M. Luckett, …, K. Gawrisch. 2004. Multinuclear NMR studies of single lipid bilayers supported in cylindrical aluminum oxide nanopores. *Langmuir.* 20:7711–7719. https://doi.org/10.1021/la0493114. https://www.ncbi.nlm.nih.gov/pubmed/15323523.

39. Straume, M., D. C. Mitchell, …, B. J. Litman. 1990. Interconversion of metarhodopsins I and II: a branched photointermediate decay model. *Biochemistry.* 29:9135–9142. https://doi.org/10.1021/bi00491a006. https://www.ncbi.nlm.nih.gov/pubmed/2271583.

40. Wald, G., and P. K. Brown. 1953. The molar extinction of rhodopsin. *J. Gen. Physiol.* 37:189–200. https://doi.org/10.1085/jgp.37.2.189. https://www.ncbi.nlm.nih.gov/pubmed/13109155.

41. Best, R. B., X. Zhu, …, A. D. MacKerell. 2012. Optimization of the additive CHARMM all-atom protein force field targeting improved sampling of the backbone phi, psi and side-chain chi(1) and chi(2) dihedral angles. *J. Chem. Theor. Comput.* 8:3257–3273. https://doi.org/10.1021/ct300400x, <Go to ISI>://WOS:000308830700029.

42. Klauda, J. B., R. M. Venable, …, R. W. Pastor. 2010. Update of the CHARMM all-atom additive force field for lipids: validation on six lipid types. *J. Phys. Chem. B.* 114:7830–7843. https://doi.org/10.1021/jp101759q, <Go to ISI>://WOS:000278479900016.

43. Salas-Estrada, L. A., N. Leioatts, …, A. Grossfield. 2018. Lipids alter rhodopsin function via ligand-like and solvent-like interactions. *Biophys. J.* 114:355–367. https://doi.org/10.1016/j.bpj.2017.11.021. https://www.ncbi.nlm.nih.gov/pubmed/29401433.

44. Jo, S., T. Kim, …, W. Im. 2008. Software news and updates - charmm-gui: a web-based grraphical user interface for CHARMM. *J. Comput. Chem.* 29:1859–1865.

45. Sodt, A. J., A. H. Beaven, …, R. W. Pastor. 2017. Gramicidin A channel formation induces local lipid redistribution II: a 3D continuum elastic model. *Biophys. J.* 112:1198–1213. https://doi.org/10.1016/j.bpj.2017.01.035. https://www.ncbi.nlm.nih.gov/pubmed/28355547.

46. Beaven, A. H., A. M. Maer, …, W. Im. 2017. Gramicidin A channel formation induces local lipid redistribution I: experiment and simulation. *Biophys. J.* 112:1185–1197. https://doi.org/10.1016/j.bpj.2017.01.028. https://www.ncbi.nlm.nih.gov/pubmed/28355546.

47. Oldfield, E., M. Meadows, …, R. Jacobs. 1978. Spectroscopic studies of specifically deuterium labeled membrane systems. Nuclear magnetic resonance investigation of the effects of cholesterol in model systems. *Biochemistry.* 17:2727–2740. https://doi.org/10.1021/bi00607a006. https://www.ncbi.nlm.nih.gov/pubmed/687560.

48. Soubias, O., W. E. Teague, Jr., …, K. Gawrisch. 2015. Rhodopsin/lipid hydrophobic matching-rhodopsin oligomerization and function. *Biophys. J.* 108:1125–1132. https://doi.org/10.1016/j.bpj.2015.01.006. https://www.ncbi.nlm.nih.gov/pubmed/25762324.

49. Phillips, R., T. Ursell, …, P. Sens. 2009. Emerging roles for lipids in shaping membrane-protein function. *Nature.* 459:379–385. https://doi.org/10.1038/nature08147. https://www.ncbi.nlm.nih.gov/pubmed/19458714.

50. Nielsen, C., M. Goulian, and O. S. Andersen. 1998. Energetics of inclusion-induced bilayer deformations. *Biophys. J.* 74:1966–1983. https://doi.org/10.1016/S0006-3495(98)77904-4. https://www.ncbi.nlm.nih.gov/pubmed/9545056.

51. Ryba, N. J., and D. Marsh. 1992. Protein rotational diffusion and lipid/protein interactions in recombinants of bovine rhodopsin with saturated diacylphosphatidylcholines of different chain lengths studied by conventional and saturation-transfer electron spin resonance. *Biochemistry.* 31:7511–7518. https://doi.org/10.1021/bi00148a011. https://www.ncbi.nlm.nih.gov/pubmed/1324716.

52. Kusumi, A., W. K. Subczynski, …, H. Merkle. 1986. Spin-label studies on phosphatidylcholine-cholesterol membranes: effects of alkyl chain length and unsaturation in the fluid phase. *Biochim. Biophys. Acta.* 854:307–317. https://doi.org/10.1016/0005-2736(86)90124-0. https://www.ncbi.nlm.nih.gov/pubmed/3002470.

53. Botelho, A. V., T. Huber, …, M. F. Brown. 2006. Curvature and hydrophobic forces drive oligomerization and modulate activity of rhodopsin in membranes. *Biophys. J.* 91:4464–4477. https://doi.org/10.1529/biophysj.106.082776. https://www.ncbi.nlm.nih.gov/pubmed/17012328.

54. Periole, X., T. Huber, …, T. P. Sakmar. 2007. G protein-coupled receptors self-assemble in dynamics simulations of model bilayers. *J. Am. Chem. Soc.* 129:10126–10132. https://doi.org/10.1021/ja0706246. https://www.ncbi.nlm.nih.gov/pubmed/17658882.

55. Kaiser, H. J., A. Orlowski, …, K. Simons. 2011. Lateral sorting in model membranes by cholesterol-mediated hydrophobic matching. *Proc. Natl. Acad. Sci. USA.* 108:16628–16633. https://doi.org/10.1073/pnas.1103742108. https://www.ncbi.nlm.nih.gov/pubmed/21930944.

56. Szundi, I., S. G. Pitch, …, D. S. Kliger. 2021. Styrene-maleic acid copolymer effects on the function of the GPCR rhodopsin in lipid nanoparticles. *Biophys. J.* 120:4337–4348. https://doi.org/10.1016/j.bpj.2021.09.012. https://www.ncbi.nlm.nih.gov/pubmed/34509506.

57. Bashkirov, P. V., K. V. Chekashkina, …, V. A. Frolov. 2011. Variation of lipid membrane composition caused by strong bending. *Biol. Membr. (Mosc.).* 28:145–152.

58. Leibler, S. 1986. Curvature instability in membranes. *J Phys-Paris.* 47:507–516.

59. Sapp, K. C., A. H. Beaven, and A. J. Sodt. 2021. Spatial extent of a single lipid's influence on bilayer mechanics. *Phys. Rev. E.* 103:042413. https://doi.org/10.1103/PhysRevE.103.042413. https://www.ncbi.nlm.nih.gov/pubmed/34005918.

60. Sarkar, P., and A. Chattopadhyay. 2022. Cholesterol in GPCR structures: prevalence and relevance. *J. Membr. Biol.* 255:99–106. https://doi.org/10.1007/s00232-021-00197-8. https://www.ncbi.nlm.nih.gov/pubmed/34365520.

61. Kumar, G. A., and A. Chattopadhyay. 2021. Membrane cholesterol regulates endocytosis and trafficking of the serotonin1A receptor: insights from acute cholesterol depletion. *Biochim. Biophys. Acta Mol. Cell Biol. Lipids.* 1866:158882. https://doi.org/10.1016/j.bbalip.2021.158882. https://www.ncbi.nlm.nih.gov/pubmed/33429076.

62. Xu, P., S. Huang, …, H. E. Xu. 2021. Structural insights into the lipid and ligand regulation of serotonin receptors. *Nature.* 592:469–473. https://doi.org/10.1038/s41586-021-03376-8. https://www.ncbi.nlm.nih.gov/pubmed/33762731.

63. Engberg, O., D. Ulbricht, …, D. Huster. 2022. Rhomboid-catalyzed intramembrane proteolysis requires hydrophobic matching with the surrounding lipid bilayer. *Sci. Adv.* 8:eabq8303. https://doi.org/10.1126/sciadv.abq8303. https://www.ncbi.nlm.nih.gov/pubmed/36149963.